Chemical Science

Accepted Manuscript

This article can be cited before page numbers have been issued, to do this please use: M. C. Gimeno, V. Fernández-Moreira and I. Marzo, *Chem. Sci.*, 2014, DOI: 10.1039/C4SC01684J.

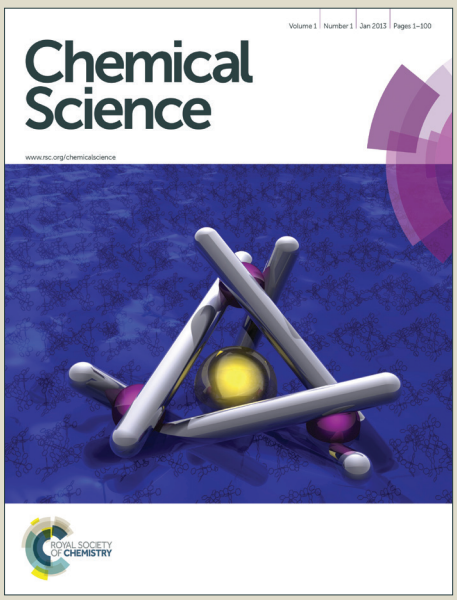

ROYAL SOCIETY OF CHEMISTRY

www.rsc.org/chemicalscience

View Article Online
DOI: 10.1039/C4SC01684J

Journal Name

RSCPublishing

ARTICLE

Luminescent Re(I) and Re(I)/Au(I) complexes as cooperative partners in cell imaging and cancer therapy

Cite this: DOI: 10.1039/xoxxoooooox

Received ooth January 2012,
Accepted ooth January 2012

DOI: 10.1039/xoxxoooooox

www.rsc.org/

Vanesa Fernández-Moreira,*[a] Isabel Marzo,[b] and M. Concepción Gimeno*[a]

A series of luminescent hometallic *fac*-[Re(bipy)(CO)3(L)]$^+$ and heterometallic *fac*-[Re(bipy)(CO)3(L-AuPPh3)]$^+$ complexes, where L is an imidazole, alkynyl-imidazole or alkynyl-pyridine derivative, have been synthesised for the purpose of finding a synergic effect between the excellent photophysical properties of rhenium complexes and the good antiproliferative effects of gold compounds. Cytotoxicity studies performed in human A549 lung cancer cells revealed the importance of the alkynyl-phosphine-gold fragment within the probe to design efficient anticancer agents. Heterometallic Re(I)/Au(I) derivatives presented values of IC50 more than 10 times lower than their analogous Re(I) complexes. In addition, fluorescent cell microscopy pointed out the different biodistribution behaviour of the monometallic and heterometallic families. Whereas the monometallic Re(I) species showed some general cytoplasmatic staining with mitochondrial accumulation, the heterometallic Re(I)/Au(I) derivatives shifted from localising in the mitochondria to the nucleus and nucleolus upon increasing the loading concentration, suggesting a completely differ rent driving force for their localisation pattern. These facts revealed that these bimetallic species can be excellent partners in cell imaging and cancer therapy.

Introduction

Several studies on gold(I) complexes have shown their anti-inflammatory activity and very recent publications also demonstrated their antitumoral, bactericidal and anti-HIV activity. Gold(I) antiarthritic drugs such as Solganol, Miocrisine, etc. and the second generation drug Auranofin®[1] have been pioneering compounds for the use of gold(I) in medicine, that has boosted the development of new metallodrugs as modern therapeutic and diagnostic agents.[2] In particular, Auranofin® is known to induce apoptosis *via* a selective inhibition of the thioredoxin reductase (TrxR), a mitochondrial enzyme. Further gold(I) complexes have shown similar behaviour, promoting the mitochondria as an extraordinary biological target for anticancer drugs.[3] One of the major features to consider in the design of novel bioactive species is their stability under physiological conditions. Within this context, gold alkynyl complexes can be thought as alternative bioactive agents to conventional gold(I) complexes. They exhibit reasonably stable coordinative bonds and the alkynyl ligand itself seems to contribute to improve the bioactivity of the species, which is of extremely importance when it comes to design anticancer agents. Several reports support the idea of an increase of the cytotoxic activity of metal complexes after introducing akynyl ligands in their coordination sphere. For instance, comparative studies on the cytotoxic effects of [Pt(terpy)Cl]$^+$ and [Pt(terpy)(C≡CAr)]$^+$ showed the latter as the species with the higher activity. Moreover, [Pt(terpy)(C≡CAr)]$^+$ turned to be about 100 times more cytotoxic than cisplatin.[4] In the particular case of alkynyl gold complexes, there have been also publications suggesting these types of organometallic compounds as a new kind of chemotherapeutic agents.[5] However, only a few studies on the biological activity of alkynyl gold compounds have been reported so far.[6]

Rhenium complexes have also attracted growing attention for their possible use as anticancer drugs.[7] To date, the studies reported in literature regarding the anticancer activity and diagnostic applications of rhenium complexes, contain derivatives of Re(I), Re(III), Re(V) and very recently Re(IV). In terms of cell visualization, species of the type [Re(bisimine)(CO)$_3$ (L)] where L is a pyridine derivative, have great potential as cell imaging agents. Their extraordinary photohysical properties,[8] *i.e.* ^{3}MLCT species with large Stokes shifts, long lifetimes and good quantum yields, have led to their successful application in fluorescent microscopy cell imaging.[9] Moreover, their kinetical inertness due to the low-spin octahedral d^6 character confers these species with a low rate of

View Article Online
DOI: 10.1039/C4SC01668D
Journal Name

ligand exchange, which is crucial in order to modulate the toxicity of heavy metal ions. Several reports on the subject have shown that a thoughtful modulation of the coordination sphere allows to tune properties such as uptake and/or localisation[10] whereas the photophysical properties remain basically unaltered. In order to take an step forward in the design of novel bioactive cell imaging agents, combination of the two metallic fragments, (a) tricarbonyl bisimine rhenium and (b) alkynyl gold species, seems to be an excellent approach to bring together photophysical properties, cytotoxic effects and bioactivity. The synergy of thoroughly selected photophysical and biological properties derived from the merging of both metallic fragments in a single species could deliver novel heterometallic species with great potential in the area of therapy and diagnosis. However, to the best of our knowledge, few examples have been published dealing with heterometallic alkynyl Re(I)/Au(I)-species, which are focused on the synthesis and photophysical properties[11] with no mention to their possible application in medicine as either therapeutic or diagnostic agents. For that reason, and with the certainty of being able to select, modulate and combine the right photophysical and biological properties by a careful design of heterometallic alkynyl Re(I)/Au(I) species, this work pretend to be the pioneer to deepen in their biological aspects. Consequently, a series of monometallic Re(I) and heterometallic alkynyl Re(I)/Au(I) were prepared and their luminescent and bioactivity properties against human A549 lung cancerous cell line were studied. Furthermore, their application as contrast agents was also analysed highlighting the importance of the partnership of the two metal centres.

Results and discussion

Synthetic procedure and characterization

The ligands **L(1-4)** used as linkers between the rhenium and gold metal centres together with their gold phosphine derivatives, **L(5-6)**, are illustrated in Fig 1. In particular, the synthesis of 2-PyC≡CAuPPh$_3$, **L5**, and 3-PyC≡CAuPPh$_3$, **L6**, has been reported elsewhere.[12] Consequently, 5-(C≡CAuPPh$_3$)ImMe, **L7**, was synthesised by a similar procedure, *i.e.* π-coordination of [AuClPPh$_3$] to the alkyne activates the terminal proton to be deprotonated by KOH in a mixture of methanol / acetone.

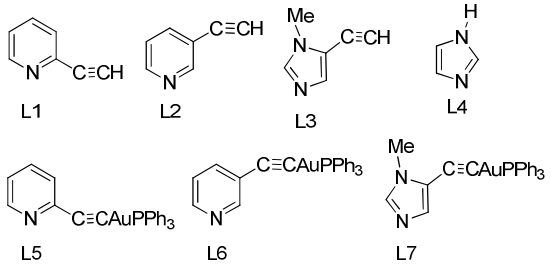

Fig. 1 Depiction of **L1-L7**.

Synthesis of complexes **1-4** and **5-8**, *i.e.* Re(I) and Re(I)/Au(I) derivatives respectively, was achieved starting from *fac*-[Re(bipy)(CO)$_3$(CF$_3$SO$_3$)] which was synthesised following literature precedents. This involved initial formation of rhenium tricarbonyl bipyridyl chloride derivative, then activation of the chloride by exchange to triflate using triflic acid affording *fac*-[Re(bipy)(CO)$_3$(CF$_3$SO$_3$)].[13] Finally, for complexes **1-3** and **5-7**, the triflate ligand was displaced for either a pyridine / imidazole derivative or their analogous gold complex under mild conditions (Scheme 1). Complex **4**, which has been already reported in the literature,[14] was also synthesized following the same procedure However, a different synthetic route was used in the synthesis of complex **8**. In this case, coordination of the gold fragment was performed directly in complex **4**, after deprotonating the imidazolyl with Cs_2CO_3 to attain **8**.

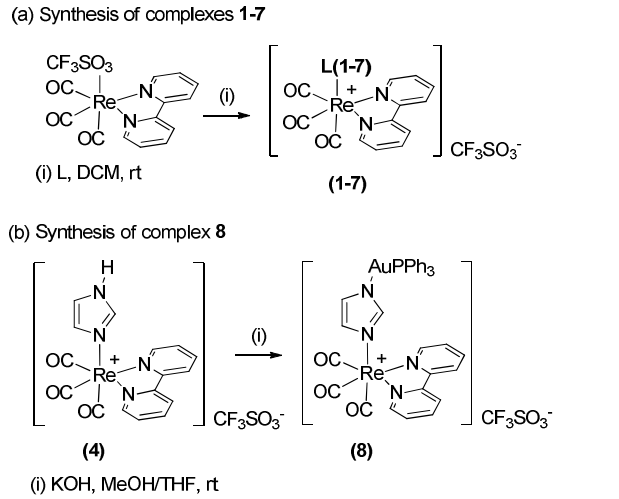

Scheme 1 Depiction of the synthesis of the monometallic and heterometalic species **1-8**.

Spectroscopic characterisation was performed using IR, ^{1}H, ^{13}C-NMR, and UV-vis spectroscopy. Further analytical data for each complex was provided through mass spectrometry, which corroborate the accomplishment on the synthesis of the mono- and heterometallic species and their purity was determined by elemental analysis. Additionally, crystals of **2, 5, 7** and **8** suitable for X-ray analysis (SHELX programs) were obtained by slow diffusion of either ether or hexane into a solution of the complex in DCM or acetone.

^{1}H-NMR spectra of complexes **1-8** were performed in either acetone-d^6 or DCM-d^2. In all cases, the spectra are well defined and exhibit the characteristic downfield shift of the bipyridine protons upon coordination to the rhenium metal centre when compared to the corresponding proton resonances of the free ligand. This phenomenon is generally rationalised in terms of the σ donation of the bipyridine ligand. Moreover, phenyl protons of the fragment -AuPPh$_3$ for the heterometallic complexes (**5-8**) are observed as multiplets in the region between 7.46 and 7.77 ppm. As a result of such coordination, there is also the disappearance of the terminal alkynyl protons in the case of **5**, **6** and **7**, which is clearly observed in their precursors at 4.82, 4.09, 4.27 ppm. Furthermore, there is an up-field shift of the protons belonging to pyridine and imidazole ligands upon coordination to the -AuPPh$_3$ fragment. Such behaviour can be interpreted in terms of π-back donation from the Au(I) centre to the

Journal Name

View Article Online
DOI: 10.1039/C4SC01684J

ligands. In addition, ^{1}H-NMR-spectroscopic data corroborate the idea of the facial disposition of CO ligands around the Re metal centre. Only four set of signals are observed in the ^{1}H-NMR spectrum for the bipyridine ligand suggesting its symmetry within the complex.[15] In the case of ^{31}P-NMR spectroscopy, a single peak appears at 41.54, 42.29, 42.19 ppm for species **5**, **6** and **7** respectively and at 31.18 ppm the case of **8**, where $AuPPh_3$ is coordinated directly to one of the nitrogen of the imidazole.[16] Such high field chemical shift of complex **8** is due to the paramagnetic shielding tensor contribution σ_{para}, which unlike in ^{1}H-NMR spectroscopy, is the main contributor to the chemical shift value. Therefore, the presence of less basic ligands in *trans* position to the P atom will promote δ_p to get shifted towards higher field than the more basic ligands.[17] Stretching frequencies of CO, C≡C and H-C≡C are selected in Table 1. The IR spectra of complexes **1-8** showed the characteristic strong ν(CO) absorptions in the range between 1892 and 2029 cm^{-1}, typical of these type of cationic species with C_{3v} symmetry around the rhenium centre, *i.e.* facial configuration.[18] In addition, complexes **5** and **6** presented a weak ν(C≡C) band in the region *of c.a.* 2122 cm^{-1}, which is typical for η^1 coordination of alkynyl gold(I) derivatives.[11b,19] Moreover, those complexes lack ν(H-C≡C) bands, which are seem for their rhenium precursors, complexes **1** and **2**.

Table 1 IR stretching frequencies for complexes **1-3** and **5-8**

Compound	ν(C≡O)	ν(C≡C)	ν(H-(C≡C)
[Au(C≡CImMe)PPh_3]	-	2159(w)	-
1	2028(s),1928(sh), 1904(s)	2113(w)	3205 (m)
2	2029(s), 1904(bs)	2113(w)	3243(m)
3	2025(s), 1918(sh), 1894(s)	-	3248(m)
5	2026(s) 1915(bs)	2123(m)	-
6	2028(s), 1903(bs)	2121(w)	-
7	2025(s), 1930(sh), 1893(s)	-	-
8	2020(s), 1921(sh), 1892(s)	-	-

X-ray crystallography

Single crystals suitable for X-ray diffraction analysis of complexes **2**, **5**, **7** and **8** were obtained by slow diffusion. Compound **2** crystallised in the monoclinic space group $P2_1/n$, and presented a single molecule in the asymmetric unit. Complexes **5**, **7** and **8** crystallised in the triclinic P-1 space group with two independent molecules in the asymmetric unit of **5** and **8**, and only one for complex **7**. The X-ray diffraction data for complex **7** is not good because of the presence of a non-solved twin crystal. Despite several attempts to recrystallise complex **7**, suitable single crystals could not be grown. Nevertheless, complex **7** will be discussed in this section together with complexes **2**, **5** and **8** although the values for the bond lengths and angles are not as accurate as for the rest of complexes. As expected, in all cases the rhenium atom presented a distorted octahedral disposition, where the carbonyl moieties adopted a facial distribution. The equatorial plane is described by the chelate bipyridine ligand and two carbonyls. The third carbonyl and the pyridine/imidazole derivative occupy the axial plane. Deviation from the ideal octahedron geometry is basically originated from the geometrical restrictions of the chelate ligand, with chelate angles of N(1)-Re(1)-N(2) = 75.28(7)º (complex **2**), N(1)-Re(1)-N(2) = 75.10(1)º and N(4)-Re(2)-N(5) = 74.50(1)º (complex **5**), N(1)-Re(1)-N(4) = 74.4(6)º (complex **7**) N(1)-Re(1)-N(2) = 74.96(13)º and N(6)-Re(2)-N(5) = 74.81(13)º (complex **8**) instead of the ideal 90º. Bond distances in the rhenium core are within the typical values for similar complexes, *i.e.* Re-C(*CO*) distances are between 1.902(3) and 1.94(3), Re-N(*py/im*) between 2.17(2) Å and 2.255(4) Å and Re-N(*Bipy*) between 2.166(2) Å and 2.19(2) Å.[20] As commented before, in the particular case of complex **5**, two independent molecules crystallised in the asymmetric unit together with their counter ion and two acetone molecules coming from the crystallisation solvent. Hydrogen bonds between either the crystallisation solvent or the counter ion with the two molecules in the asymmetric units are also present, with distances ranging from 2.487Å to 2.641Å (Fig. S1 and Fig. S2). Likewise, complex **8** has two independent molecules within the asymmetric unit, which crystallises with their corresponding counter ions and an ether molecule from the crystallisation solvent. Molecule 1 presents a short contact between one of the oxygen atoms from the triflate and a hydrogen atom from the phenyl ring (O(12)···H(25) = 2.668 Å), which can be considered as a hydrogen bond (Fig. S3).

In addition, heterometallic species, complex **5, 7** and **8**, presented the gold atom in a distorted linear geometry with C-Au-P angles of *c.a.* 174° for complexes **5** and **7** and an angle of N-Au-P of *c.a.* 177° for complex **8**. Bond distances within the gold environment are also within the normal values for C≡C-Au-P derivatives and Im-Au-P.[12a,16,21] A summary of bond distances and angles is presented in Figs. 2-5.

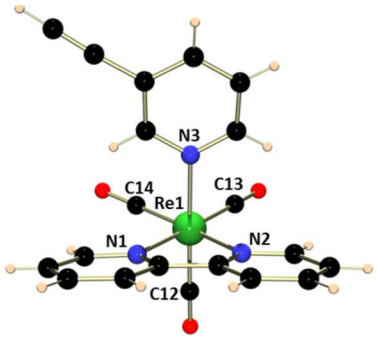

Fig. 2 Ortep representation of complex **2**. The most relevant bond lengths (Å) and angles (deg): Re(1)–C(12) = 1.932(2), Re(1)–C(13) = 1.934(2), Re(1)–C(14) = 1.902(3), Re(1)–N(1) = 2.166(2), Re(1)–N(2) = 2.172(2), Re(1)–N(3) = 2.214(2); N(1)–Re(1)–N(2) = 75.28(3), C(12)–Re(1)–N(3) = 174.40(9).

View Article Online
DOI: 10.1039/C4SC01668D
Journal Name

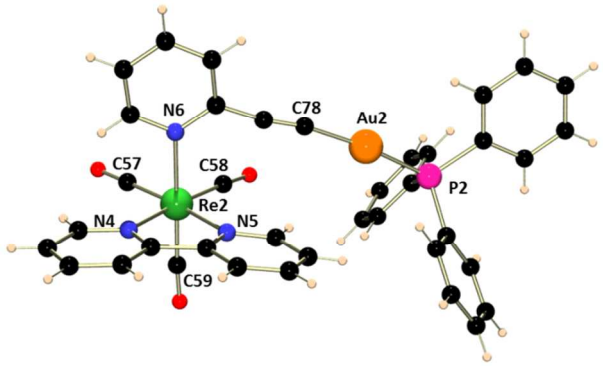

Fig. 3 Ortep representation of complex **5**. Re(2)–C(57) = 1.919(5), Re(2)–C(58) = 1.919(5), Re(2)–C(59) = 1.909(5), Re(2)–N(4) = 2.174(3), Re(2)–N(5) = 2.174(4), Re(2)–N(6) = 2.242(4); N(5)–Re(2)–N(4) = 74.5(1), N(6)–Re(2)–C(59) = 176.7(2), Au(2)–C(78) = 1.995(5), Au(2)–P(2) = 2.278(1).

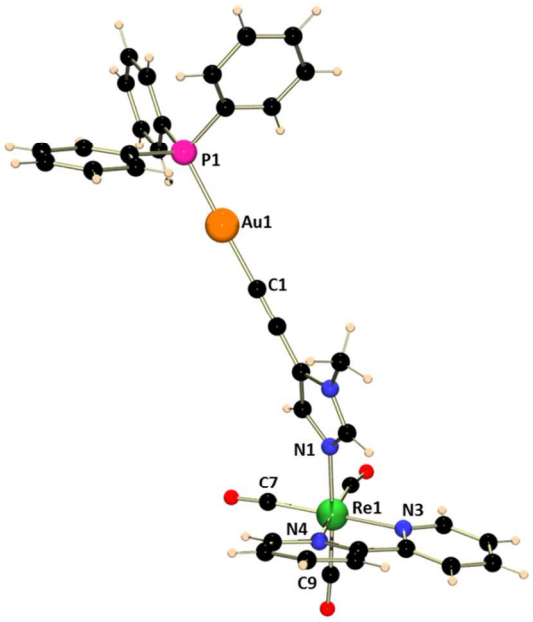

Fig. 4 Ortep representation of complex **7**. The most relevant bond lengths (Å) and angles (deg): Re(1)–C(7) = 1.92(2), Re(1)–C(8) = 1.94(3), Re(1)–C(9) = 1.91(2), Re(1)–N(3) = 2.18(2), Re(1)–N(4) = 2.19(2), Re(1)–N(1) = 2.17(2); N(4)–Re(1)–N(1) = 74.4(6), C(9)–Re(1)–N(1) = 176.5(7), P(1)–Au(1)–C(1) = 173.85, Au(1)–C(1) = 2.00(1), Au(1)–P(1) = 2.27(4).

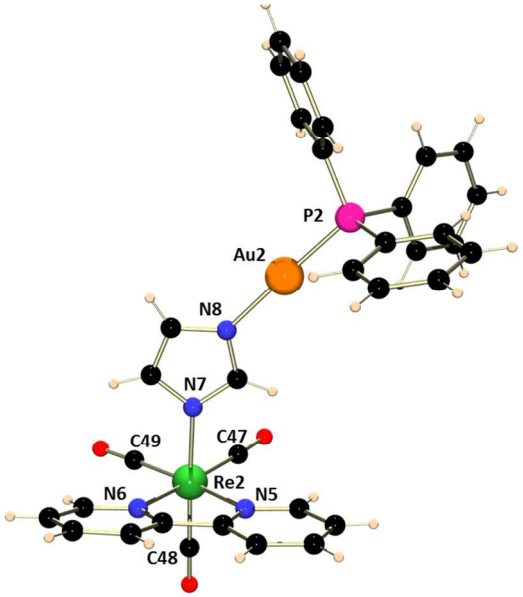

Fig. 5 Ortep representation of complex **8**. The most relevant bond lengths (Å) and angles (deg): Re(2)–C(47) = 1.932(4), Re(2)–C(48) = 1.929(5), Re(2)–C(49) = 1.915(4), Re(2)–N(6) = 2.169(3), Re(2)–N(7) = 2.175(3), Re(2)–N(5) = 2.181(3), N(5)–Re(2)–N(6) = 74.8(1), N(7)–Re(2)–C(48) = 178.3(2), P(2)–Au(2)–N(8) = 177.9(1), Au(2)–N(8) = 2.048(4), Au(2)–P(2) = 2.235(1).

Photophysical studies

UV-visible absorption spectra, recorded in a degassed CH_3CN solution at 298K, show the typical pattern for bisimine Re(I) derivatives (Fig. 6 and Fig. S4). There are ligand centred transitions (alkynyl, bipyridine, pyridine and imidazole derivatives) at higher energies, $\pi \rightarrow \pi^*$ transitions at < 320 nm, and metal-to-ligand-charge-transfer transitions (^{1}MLCT), formally attributed to Re(dπ) $\rightarrow$ L(π^*) transitions, at lower energies 352 - 366 nm, with a tail extending up to 420 nm. Moreover, it is noteworthy that heterometallic species have a considerable increment in the molar extinction coefficient for the $\pi \rightarrow \pi^*$ bands in comparison with the monometallic analogue. Such difference could be associated with the existence of an intense absorption at *c.a.* 288 nm, which appears depending on the alkynyl ligand present and it is likely assigned as a mixture of intraligand $\pi \rightarrow \pi^*$ (C≡C) , $\pi \rightarrow \pi^*$ (bipy) and $\pi \rightarrow \pi^*$ (PPh_3) transitions.[11a] On the contrary, molar extinction coefficients for the ^{1}MLCT bands are practically the same. Such behaviour could be attributed to the fact that the main ligand orbital implicated in the MLCT transition is that belonging to the bipyridine ligand. Specifically the ^{1}MLCT transition is a Re(dπ) $\rightarrow$ bipy(π^*) transition, which remains unaltered by the coordination of the gold fragment to either a pyridine or a imidazole fragment. The most significant absorption data together with the emission maxima values for all complexes are collected in Table 2.

View Article Online
DOI: 10.1039/C4SC01684J

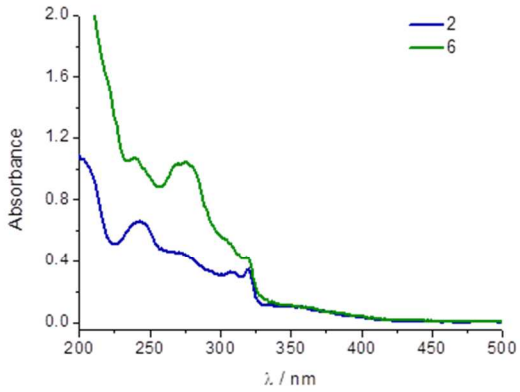

Fig. 6 UV-absorption spectra of complexes **2** and **6** recorded in degassed CH_3CN at 298 K.

Table 2 Absorption bands, excitation and emission maxima values.

species	UV-Vis ($\times 10^4$ ε/dm^{3}mol^{-1}cm^{-1})				λ_{exc} (nm)	λ_{em} (nm)
1	240 (2.28)	277 (1.82)	321 (1.20)	357 (0.51)	398	577
2	236 (3.04)	268 (1.40)	318 (0.94)	360 (0.32)	404	574
3	242 (2.49)	276 (1.36)	318 (1.08)	352 (0.38)	412	604
4	248 (1.20)		318 (1.07)	356 (0.34)	417	600
5	243 (3.98)	265 (2.91)	305 (2.16)	366 (0.34)	400	592
6	240 (4.26)	278 (4.16)	3.19 (1.68)	357 (0.37)	400	576
7	237 (4.45)	271 (3.42)	318 (1.10)	352 (0.33)	402	607
8	237 (3.04)		318 (0.94)	356 (0.31)	410	628

Degassed CH_3CN, 298 K

Luminescence spectra of complexes (**1-4**) and (**5-8**) were recorded in degassed CH_3CN solution at 298 K (Fig 7 and Fig S6). All of them showed a broad emission between 577 - 628 nm which is attributed to the phosphorescence from the Re(dπ) → bipy(π*) ^{3}MLCT excited state and it has been previously reported in many rhenium(I) diimine tricarbonyl complexes.[8, 22] It is interesting to note, that emission of 2-PyC≡CAuPPh$_3$, **L5**, which has been already studied in our group[12b] and with a maximum at 450 nm, does not appear when this fragment is coordinated to [Re(bipy)(CO)$_3$CF$_3$SO$_3$] to give **5**. Such behaviour could be interpreted as an efficient of intramolecular energy transfer process from the Au(I) unit to the Re(I) unit, specifically from the ^{3}[σ(Au-P)→π*(C≡CR)] to the lower-lying ^{3}MLCT ^{3}[dπ(Re)→π*(bipy)] excited state and it is in agreement with optical studies of analogous mixed gold(I)-rhenium(I) complexes performed by Yam and coworkers.[11a] Luminescent lifetime measurements have been performed for the Re complexes **2** and **3**, and for the corresponding mixed Re-Au species **6** and **7** in degassed CH_3CN solution. They present values from 40.15 to 148 ns, with very similar values within the Re and the corresponding Re-Au species. For example for the rhenium complex **2** the lifetime is 148 ns and for the corresponding rhenium-gold **6**, 134 ns. Similarly, **3** presents a value of 52.56 ns and **7** of 40.15 ns. The similarity within the Re and the corresponding Re-Au species lifetime values, together with those reported in the literature for rhenium complexes point out that the origin of the emission in the complexes is mainly due to the Re species and not to the gold alkyne fragment, which agrees with the experimental data. [10a,18b]

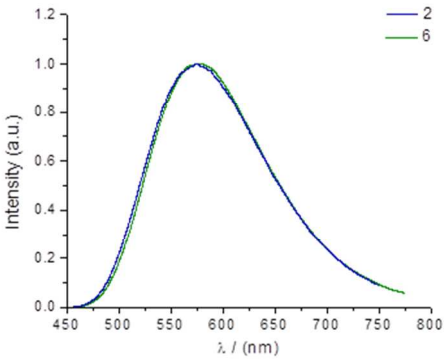

Fig. 7 Emission spectra of complexes **2** and **6** recorded in degassed CH_3CN at 298 K, excitation at 404 and 400 nm, respectively.

Cellular studies and fluorescence microscopy

In view of the favourable emissions properties of complexes **1-8**, and of the good stability in solution of both the rhenium and the rhenium-gold complexes, as the ^{1}H and ^{31}P NMR signals remain the same with time, a series of experiments were undertaken to test their cytotoxicity and viability as contrast agents in human A549 lung carcinoma cells. As commented before the gold-alkynyl bond is amongst the strongest Au-ligand bonds, the same happen with the Au-P bond. Study of the cytotoxic effect was performed by an annexin-V analysis and revealed a great cytotoxic difference between the heterometallic (**4-8**) and monometallic complexes (**1-4**). Table 3 summarises the IC_{50} found for all complexes pointing out the higher cytotoxicity of heterometallic species in comparison with their rhenium analogues.

Table 3 Values of IC_{50} for species **1-8**

Monometallic:	**1**	**2**	**3**	**4**
IC_{50} (μM)	120±29	200±56	-	-
Heterometallic:	**5**	**6**	**7**	**8**
IC_{50} (μM)	9.5±1.0	9.7±1.1	4.4±0.5	19±7.9

Whereas complexes **1-4** showed IC_{50} values over 100 μM and even some of them did not seem to be cytotoxic at the studied concentrations, the heterometallic complexes **5-8** presented IC_{50} values lower than 20 μM. Such cytotoxic difference between the monometallic and the heterometallic species might be associated with the role of Au-phosphine fragment rather than a synergic effect with the [Re(bipy)(CO)$_3$L] core. The probed cytotoxic activity of different gold(I) phosphine fragments reported on several cell lines supports this idea.[6,23] The

cytotoxic activity in A549 cells have been reported only for a few gold(I) complexes, and none of them in the same conditions that those reported here. Auranofin gives a value of 0.72 μM after 72 h of incubation for the MTT method, but this value could be considerably higher at 24 h.[3f] We have reported values as low as 0.4 μM after 24 h of incubation for the MTT method for a thiazolylalanine carbene gold species.[24] These facts probes that cytotoxic activity comes mainly from the gold fragment rather than the rhenium moiety.

A closer look to this result revealed that among the monometallic complexes those bearing an imidazole derivative are the least cytotoxic species, *i.e.* complexes **3** and **4**. In contrast, among the heterometallic complexes, those having an alkynyl in their chemical structure turned to be the most cytotoxic species reaching IC_{50} values of even as low as 4 μM, (Fig. 8 and Fig. S5).

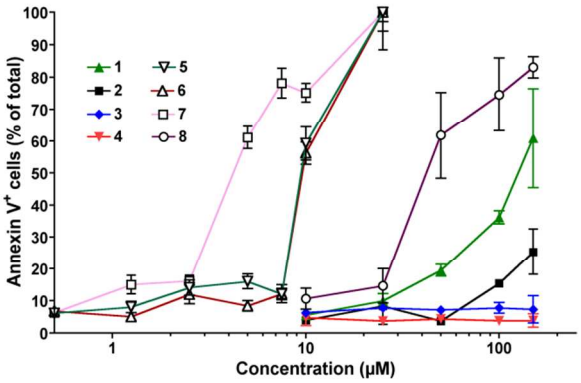

Fig. 8 Representation of toxicity values of complexes **1-8** obtained by annexin-V analysis.

This result is in concordance with the idea that the presence of alkynyl groups increases the cytotoxic activity of the probe.[4] In addition, examination of the cell morphology suggested that cellular death might be due to apoptosis for species **1** and **2**, with cell shrinking and blebbing. For species **3**-**4** and **5**-**8** some apoptotic cells can be observed but cellular death could be due to both apoptosis and necrosis (Fig. S6)**.**

In an attempt to assess whether these complexes could be used as contrast agents, they were incubated with A549 lung carcinoma cells and their emission was examined by fluorescent confocal microscopy. Complexes were loaded at concentrations below their IC_{50} values, *i.e.* monometallic species **1**-**4** at 150 μM and complexes **5**-**8** at 10, 10, 5 and 15 μM respectively. In addition, a known DNA co-staining fluorescent dye, DRAQ5, was used as an internal standard in order to ascertain the site of cellular localisation. Confocal fluorescent images were taken after excitation at 405 nm and 647 nm. Using a 405 nm laser excitation, only emission from the complexes **1**-**8** was observed, whereas exciting at 647 nm the emission displayed was that of the known fluorescent dye localised in the nucleus, where the DNA is concentrated. Therefore, upon excitation at 405 nm cells incubated with complexes **1**-**4** showed an emission coming from almost all the cell region with more intensive luminescence in specific spots within the cytoplasm, (Fig. 9). Such, distinct granular localization pattern might be indicative of mitochondrial staining. The only area in the cell that seems not to uptake the complexes resembles that of the nucleus. Superimposition of the images obtained upon excitation at 405 nm and 647 nm gave crucial information to elucidate the possible localisation pattern. Hence, (Fig. 9A) clearly showed as complexes **1**-**4** were taken up by the cell (red colour), with an emission coming from the cytoplasmatic area except for the nucleus, which is lighted up in blue due to the specific staining of DRAQ5, (Fig 9B). Such localisation pattern has been previously seen for several tricarbonyl bisimine rhenium derivatives and it is the typical localisation of monocationic Re complexes; some general cytoplasmatic staining with more intense mitochondrial localisation and no emission from the nucleus.[10(a-c),25] Negligible emission from the nuclei indicates the exclusion of the complexes from the nucleous, which seems to be also an common feature for monocationic Re complexes.[10f,26]

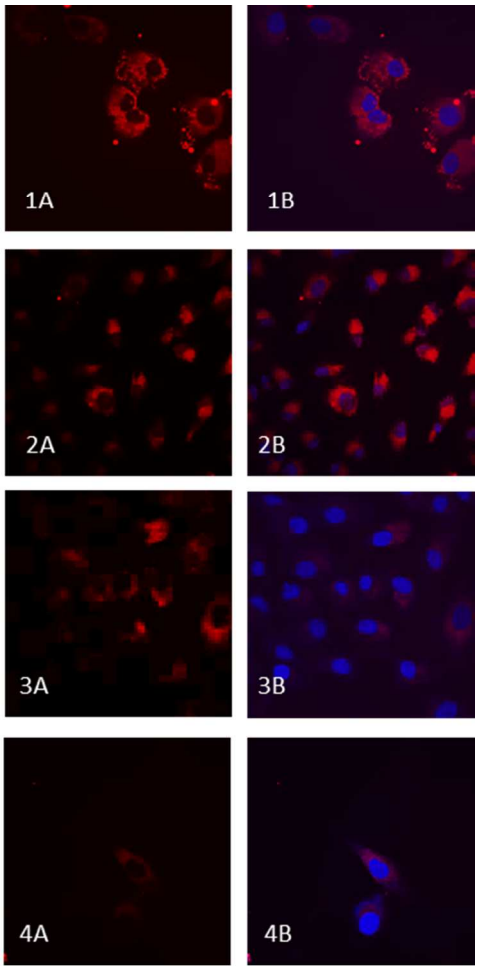

Fig. 9 Images of complexes **1**-**4** incubated with A549 cells for 4 h at 150 μM. (A) Images upon excitation at 405 nm. (B) Superimposed image upon excitation at 405 nm and 647 nm. Please note that images from complex **2** and **3** were taken with an objective of ×10 which might lower the resolution of the picture.

Journal Name
View Article Online
DOI: 10.1039/C4SC01684J
ARTICLE

Heterometallic species **5-8** showed a similar pattern to that of monometallic species, with the strongest luminescence emission coming from specific spots in the cytoplasm and none of complexes seemed to enter the nucleus either, (Fig 10). Several factors within these species, such as their cationic nature, their lipophilicity and being thiol and selenol reactive because of the presence of gold(I), point out the possibility of considering the mitochondria as the possible target. Comparison with published reports of Au(I) complexes supports the mitochondrial localisation hypothesis, as cancerous cells bear an elevated expression of thioredoxin reductase which is known to be inhibited by Au(I) species.[27] It is worth pointing out that even though the loading concentration was much lower for the heterometallic species, the emission intensity was similar, which is an indication of the ease internalization of the dye. Consequently, it could be rationalised that the fragment $-AuPPh_3$ confers higher lipophilicity to the probe, and facilitates the cell membrane permeability.

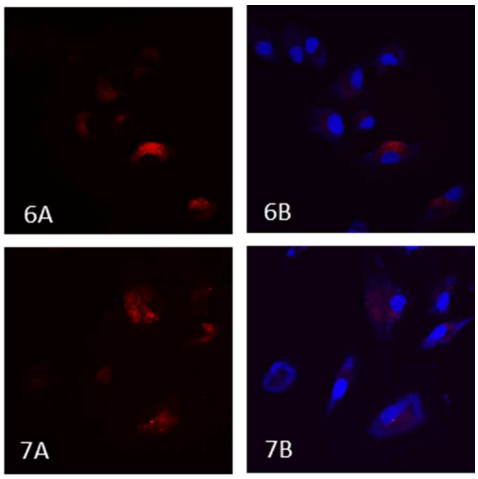

Fig. 10 Images of complexes **6-7** incubated with A549 cells for 4 h at 150 µM. (A) Images upon excitation at 405 nm. (B) Superimposed image upon excitation at 405 nm and 647 nm.

Finally, the cell imaging assay of the heterometallic species **5-8** was repeated using the same loading concentration as in the case of monometallic species **1-4**, *i.e.* 150 µM**.** The aim of this new experiment was to make a fair comparison between both set of complexes regarding their uptake level as well as to analyse the possibility of another localisation pattern. Indeed, all of them revealed a completely different behaviour than the previously observed (Fig. 11). Complexes **5-7**, *i.e.* the heterometallic species bearing an alkynyl group, presented higher internalisation than the monometallic analogues **1-4,** and also than the mixed Re(I)/Au(I) complex lacking of alkynyl, complex **8**. The laser power for visualising the cells incubated with those alkynyl heterometallic derivatives (**5-7**) had to be lowered from 40% to *c.a.* 2% in order not to damage the detector, which revealed their higher concentration in the cell. Such result**,** suggested some sort of relationship between cellular uptake and heterometallic akynyl derivatives.

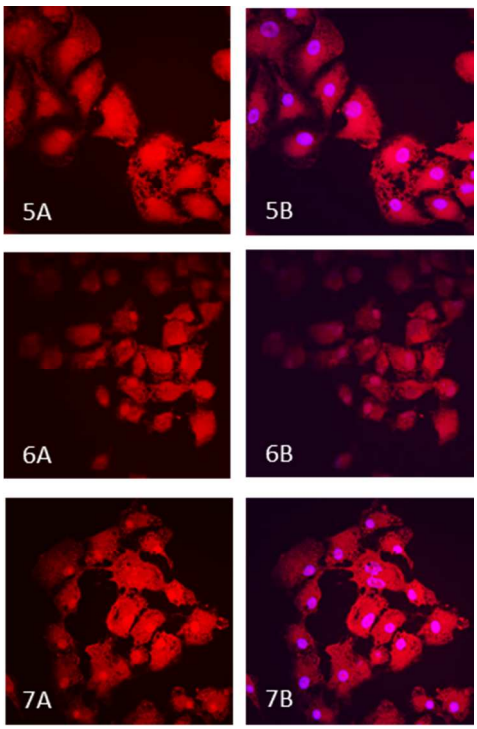

Fig. 11 Images of complexes **5-7** incubated with A549 cells for 4 h at 10, 10 and 4 µM respectively. (A) Images upon excitation at 405 nm. (B) Superimposed image upon excitation at 405 nm and 647 nm.

Moreover, these heterometallic species bearing an alkynyl group, complexes **5-7**, seemed to present a different localisation pattern than this lacking of an alkynyl group, complex **8** (Fig 12). Therefore, complex **8** showed emission spread out along the cell including the nucleus whereas complexes **5-7** apart from displaying an emission dispersed all along the cell, seemed to accumulate in a specific organelle in the nucleus.

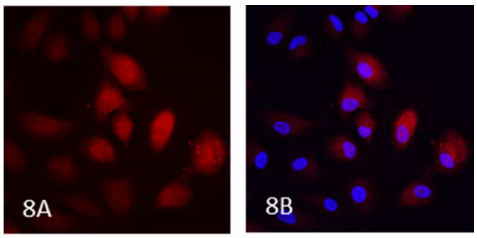

Fig. 12 Images of complexes **8** incubated with A549 cells for 4 h at 15 µM respectively. (A) Images upon excitation at 405 nm. (B) Superimposed image upon excitation at 405 nm and 647 nm.

The superimposed image of Fig. 11B revealed a clear overlap of the red emission belonging to species **5-7** with the blue emission coming from DRAQ5, which is a clear indication of the nuclear staining. Moreover, a closer look to an amplified image revealed that complexes **5-7** not only get accumulated in the nucleus but also, they seem to localise preferentially in an area inside the nucleus that it is assumed to be the nucleolus (Fig. 13).

View Article Online
DOI: 10.1039/C4SC01664D
Journal Name

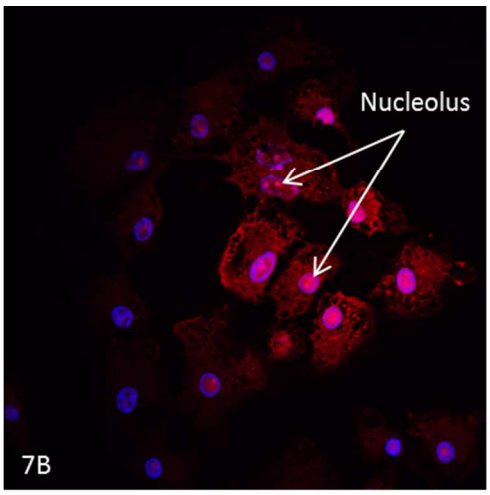

Fig. 13 Amplified image of complex **7** (red colour: emission from the synthesised complexes, blue colour: emission from DRAQ5).

On the other hand, complex **8** seemed to behave in an intermediate manner between the monometallic (**1-4**) and heterometallic alkynyl derivatives (**5-7**) as the internalisation level is similar to that seen for complexes **1-4** but instead its localisation pattern resembles to that of species **5-7**. Hence, complex **8** exhibited a luminescence spread over the cell, including the nucleus, although no clear accumulation of the probe seems to take place in the nucleolus (see Fig 12). In an attempt to shed a bit of light to the behaviour of complexes **1-8** incubated with A549 cells, the integrity of the cell membrane was analysed by a cell viability test. Trypan blue, a dye widely used for selective staining of dead tissues or cells, was added after incubation in A549 cells for 4 h. Fig. 14 shows that cells incubated with complexes **5-8** at concentrations of 150 μM allowed Trypan blue to cross the cell membrane, which is an indication of membrane permeabilisation. In contrast, cell incubated with complexes **1-4** at the same concentration remained healthy.

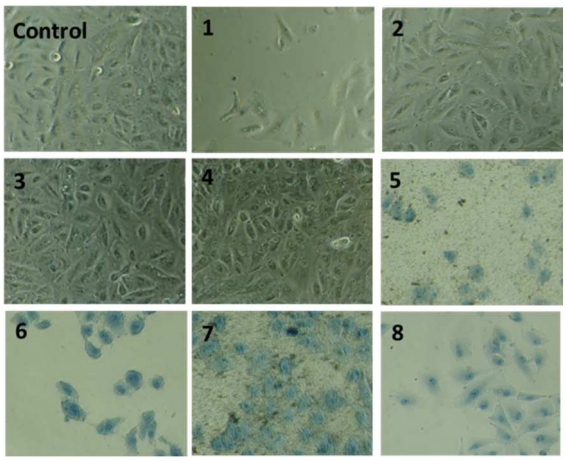

Fig. 14 Cell viability test (Blue colour: emission from Trypan blue indicating that the cell membrane has been disrupted upon incubation with the different complexes.

The presence or absence of an alkynyl moiety in the ligand structure, did not affect these results, proposing the heterometallic character as the key point for the membrane permeabilisation. Such analysis agrees with the cytotoxicity levels found for each complex, being the heterometallic complexes **5-8** those with the lowest IC_{50} values. Hence, in view of these results, it can be proposed that the higher toxicity might promote the disruption of the cellular membrane and in consequence those probes get internalized easily, *i.e.* species **5-7**. Moreover, it is also worth mentioning that all of them bear the fragment $–AuPPh_3$, which should increase the lipophilicity of the probe. In addition, species **8**, the only synthesized heterometallic species lacking of an alkynyl group and the less cytotoxic (IC_{50} of 19 μM), does not have the same level of internalisation as their analogous complexes **5-7**, but its localisation pattern is alike. Such findings go along with the idea that the localisation pattern could be related to the presence of the fragment $–AuPPh_3$. Some examples published by Ott and coworkers on naphthalimide phophine gold derivatives as anticancer metallodrugs, emphasises that uptake increases upon exposure to toxic concentrations as it is supposed to be associated with a breakdown of the cell membrane integrity.[28] They observed that localisation of those gold phosphine derivatives is preferably in the cell nuclei, which is the same behaviour displayed by complexes **5-8**. Further investigations on the bio-activity of alkynyl phosphine gold derivatives also suggest the fragment $–AuPPh_3$ as the responsible to bring the molecules to the site of action within the cell.[6f] This rationalization together with the high toxicity associated with these species might explain the reason why the heterometallic complexes **5-8** have a different localisation pattern than complexes **1-4**. In addition to these examples on gold complexes in cell imaging, some others metallic bioprobes such as luminescent lanthanide complexes published by Parker and co-workers pointed out that disrupting the cell permeability with surfactants or increasing the probe concentration or incubation times induce localisation in the nucleoli and ribosomes.[29] They also demonstrated that localisation patterns can be influenced by the loading concentration. Consequently, some reported lanthanide species incubated at concentration beyond their IC_{50} revealed nucleolar staining, whereas incubation of those at lower concentration presented a different pattern.[30] These findings completely agrees with the behaviour seem for the heterometallic complexes described in here, complexes **5-8**, corroborating their nucleolar localisation. It is worth mentioning that although the highest level emission of complexes **5-7** is coming from the nucleus and nucleolus, there is also a weak luminescence throughout the entire cell. Such luminescence spread over the entire cell was observed as well in some alkynyl phosphine gold complexes reported by Dyson and coworkers.[6d] In this case, the low fluorescence intensity observed prevented the subcellular compartment from being identified. This drawback has been overcome in the present publications with the synthesis of heterometallic Re(I)/Au(I)-species, where the Re fragment is assisting to increase the

View Article Online
DOI: 10.1039/C4SC01684J

luminescence intensity whereas the Au fragment is controlling the main biological aspects, *i.e.* localisation and cytotoxicity.

Experimental

General Measurements and Analysis Instrumentation

C, H, and N analysis were carried out with a PERKIN-ELMER 2400 microanalyzer. Mass spectra were recorded on a BRUKER ESQUIRE 3000 PLUS, with the electrospray (ESI) technique and on a BRUKER (MALDI-TOF). ^{1}H, ^{13}C{H} and ^{31}P NMR, including 2D experiments, were recorded at room temperature on a BRUKER AVANCE 400 spectrometer (^{1}H, 400 MHz, ^{13}C, 100.6 MHz, ^{31}P, 162 MHz) with chemical shifts (δ, ppm) reported relative to the solvent peaks of the deuterated solvent. Infrared spectra were recorded in the range 4000–250 cm^{-1} on a Perkin-Elmer Spectrum 100 FTIR spectrometer. Room temperature steady-state emission and excitation spectra were recorded with a Jobin-Yvon-Horiba fluorolog FL3-11 spectrometer fitted with a JY TBX picosecond detection module. Lifetime measurements were recorded with a Datastation HUB-B with a nanoLED controller and DAS6 software. The nanoLED employed for lifetime measurements was one of 390 nm with pulse lengths of 0.8–1.4 ns. The lifetime data were fitted with the Jobin-Yvon software package. UV/vis spectra were recorded with a 1cm quartz cells on an Evolution 600 spectrophotometer.

Crystal Structure Determinations.

Crystals were mounted in inert oil on glass fibers and transferred to the cold gas stream of an Xcalibur Oxford Diffraction diffractometer equipped with a low-temperature attachment. Data were collected using monochromated MoKα radiation (λ= 0.71073 Å). Scan type ω. Absorption correction based on multiple scans were applied using spherical harmonics implemented in SCALE3 ABSPACK scaling algorithm. The structures were solved by direct methods and refined on F^2 using the program SHELXL-97.[31] All non-hydrogen atoms were refined anisotropically, with the exception of complex **7**. Further details on the crystal refinements are collected in Table 4.

Human Cell Studies and Cell Microscopy.

European Collection of Cell Cultures, were maintained in Hepes modified minimum essential medium (HMEM) supplemented with 10% fetal bovine serum, penicillin, and streptomycin. Cells were detached from the plastic flask using trypsin-EDTA solution and suspended in an excess volume of growth medium. The homogeneous cell suspension was then distributed into 1 mL aliquots over a cover slip in a 24-well plate, with each aliquot being subject to incubation with the different complexes, final concentrations varies from 125 μM to 4 μM, at 37 °C for 4 h. Cells were finally washed three times in phosphate buffer saline (PBS, pH 7.2). Then, 0.5 ml of paraformaldehyde 4% was added to fix the cells at 37 °C for 15 min. Eventually, cells were washed three times with phosphate buffer saline (PBS, pH 7) and they were mounted on a slide for imaging where previously was added 5μl of Flouromont and DRAQ5 (1, 5-bis-[2-(di-methylamino)ethyl]amino]-4, 8-dihydroxyanthracene-9,10-dione) (2 μM). Preparations were viewed using an Olympus FV10-i Oil type compact confocal laser microscope using an ×10 or ×60 objective, with excitation wavelength at 405 nm and 647 nm.

The integrity of the plasmatic membrane was analysed by the Trypan-blue exclusion test. Cells were treated for 4 h with compounds **1-8** at a concentration of 150 μM in 24-well plates. Then, 50 μL of Trypan blue solution (0.4 % w/v in NaCl 0.15 M) were added to wells and cells were observed and photographed in an optical microscope at 400x magnification.

Cell death after treatment with compounds **1-8** was analysed by measuring exposure of phosphatidylserine. Cells were treated for 24 h with different concentrations (0.1-150 μM) of compounds. Cell morphology after treatment with compounds was evaluated by optical microscopy (400 x magnification) and representative fields were photographed. Then, cells were trypsinized and incubated at 37ºC for 15 minutes in ABB (140 mM NaCl, 2.5 mM $CaCl_2$, 10 mM Hepes / NaOH, pH 7.4) containing 0.5 μg/ml AnnexinV-PE. Finally, cells were diluted to 0.5 ml with ABB and analysed by flow cytometry (FACScan, BD Bioscience, Spain).

Materials and Procedures

The intermediate *fac*-[Re(bipy)(CO)$_3$(CF$_3$SO$_3$)] was prepared according to literature procedures.[12b,c] Complex **4**, specifically *fac*-[Re(bipy)(CO)$_3$(ImH)](CF$_3$SO$_3$), has been prepared using a modified method to that one reported in the literature for the synthesis of the analogous hexafluorophospate salts,[13] see below. All other starting materials and solvents were purchased from commercial suppliers and used as received unless otherwise stated.

[Au(C≡CImMe)PPh$_3$]: 5-ethynyl-1-methyl-1H-imidazole (36 μl, 0.35 mmol) and KOH (59 mg, 1.05 mmol) were stirred in methanol (5 ml) for 5 minutes under an argon atmosphere. Then, [AuClPPh$_3$] (183 mg, 0.37 mmol) dissolved in a mixture of methanol acetone (1:1) was added and the reaction was kept stirring for 12 hours. The white solid precipitated was filtered and washed with further methanol to furnish 140 mg, 75 % yield. ^{1}H NMR (400 MHz, Acetone) δ 7.69-7.55 (m, 15H, 3Ph), 7.47 (s, 1H C*H*(2) Im), 6.93 (d, *J* = 1.0 Hz, 1H,C*H*(4) Im), 3.65 (s, 3H, C*H*(Me)).). ^{31}P NMR (162 MHz, Acetone) δ 42.46. ^{13}C NMR (101 MHz, Acetone) δ 137.9 (*C*(2)), 134.9 (d, ^{2}J = 13.1 Hz, C*ortho*, Ph), 132.7 (d, ^{4}J = 2.4 Hz, C*para*, Ph), 132.3 (*C*(4)), 130.8 (*C*(C*C*Au-)), 133.3(d, ^{3}J = 11.3 Hz, C*meta*, Ph), 119.1 (*C*(5)), 90.1 (*C*(*C*CAu-)), 31.9 (*C*(Me)). C*ipso*(Ph) not observed. IR (solid, cm^{-1}): 2159w (C≡C), MS ES *m/z*: calculated for $C_{24}H_{20}AuN_2P$ (M^+) 564.1, found 565.2 (MH)

Complex 1: A solution of [Re(bipy)(CO)$_3$(CF$_3$SO$_3$)] (100 mg, 0.17 mmol) and 2-PyC≡CH (72 μl, 0.68 mmol) in DCM (3 ml) were stirred for 5 days at room temperature under an argon atmosphere. Then, addition of ether afforded the precipitation of a dark brown gel which was separated by decantation. Finally, a trituration process with ether afforded complex **1** as light brown solid (32 mg, 27 % yield). ^{1}H NMR (400 MHz, Acetone) δ 9.56 (ddd, *J* = 5.5, 1.5, 0.7 Hz, 2H, C*H*(6) bipy), 8.73 (d, *J* = 8.2 Hz, 2H C*H*(3) bipy), 8.49 – 8.41 (m, 3H C*H*(4) bipy, C*H*(6) Py), 8.03 – 7.94 (m, 3H, C*H*(5) bipy, C*H*(4) Py), 7.77 (ddd, *J* = 7.9, 1.5, 0.7 Hz, 1H, C*H*(3) Py), 7.42 (ddd, *J* =

DOI: 10.1039/C4SC01684D

7.5, 5.9, 1.6 Hz, 1H, C*H*(5) Py), 4.82 (s, 1H, CC*H*). ^{13}C NMR (101 MHz, Acetone) δ, 196.3 (*C*O), 191.8(*C*O), 157.1 (*C*(2) bipy), 156.4 (*C*(6) bipy), 153.6 (*C*(6) py), 146.3 (*C*(2) py), 142.34(*C*(4) bipy), 140.9(*C*(4) py), 133.4(*C*(3) py), 129.3 (*C*(5) bipy), 127.1(*C*(5) py), 125.6(*C*(3) bipy), 91.8 (*CC*H), 82.6 (*C*CH). IR (solid, cm^{-1}): 2028s (CO), 1928sh (CO), 1904s (CO), 2113w (C≡C), 3205m (H-CC), MS ES *m/z*: calculated for $C_{20}H_{13}N_3O_3Re^+$ (M^+) 530.1, found 529.8.

Complex 2: [Re(bipy)(CO)$_3$(CF$_3$SO$_3$)] (200 mg, 0.34 mmol) and 3-PyC≡CH (118 mg, 1.14 mmol) were stirred in DCM (15 ml) for 12 h at room temperature under an argon atmosphere. Then, the volume of the reaction was reduced up to 1/3 under vacuum and ether was added affording the precipitation of **2** as a yellow solid (135 mg, 57 % yield). ^{1}H NMR (400 MHz, Acetone) δ 9.52 (ddd, *J* = 5.5, 1.4, 0.7 Hz, 2H, C*H*(6) bipy), 8.78 (d, *J* = 8.2 Hz, 2H, C*H*(3) bipy), 8.63 – 8.61 (m, 1H, C*H*(2) py), 8.57 (dd, *J* = 5.7, 1.0 Hz, 1H, C*H*(6) py), 8.48 (td, *J* = 8.0, 1.5 Hz, 2H, C*H*(4) bipy), 8.09 – 8.05 (m, 1H, C*H*(4) py), 8.02 (ddd, *J* = 7.7, 5.5, 1.2 Hz, 2H, C*H*(5) bipy), 7.52 (ddd, *J* = 8.0, 5.7, 0.7 Hz, 1H, C*H*(5) Py), 4.09 (s, 1H, CC*H*). ^{13}C NMR (101 MHz, Acetone) δ 196.1 (*C*O), 192.3 (*C*O), 156.9 (*C*(2) bipy), 155.2 (*C*(2) py), 155.0 (*C*(6) bipy), 152.7 (*C*(6) py), 143.7 (*C*(4) py), 142.4 (*C*(4) bipy), 130.0 (*C*(5) bipy), 127.7 (*C*(5) py), 126.0 (*C*(3) bipy), 123.2 (*C*(3) py), 85.5 (C*C*H), 78.4 (*C*CH). IR (solid, cm^{-1}, ν(CO)): 2029, 1904, MS ES *m/z*: calculated for $C_{20}H_{13}N_3O_3Re^+$ (M^+) 530.0, found 530.2. Elemental analysis for $C_{21}H_{13}F_3N_3O_6ReS$ required C, 37.17; H, 1.93; N, 6.19 %, found C, 37.25; H, 2.27; N, 6.24 %.

Complex 3: To a solution of 5-ethynyl-1-methyl-1*H*-imidazole (0.176 ml, 1.73 mmol) in dry DCM (15 ml) was added [Re(bipy)(CO)$_3$(CF$_3$SO$_3$)] (100 mg, 0.17 mmol) affording a brown-orange suspension. The suspension was stirring at room temperature under an argon atmosphere for 12 hours. Then, the volume of the solution was reduced up to 2/3 and ether was added dropwise to give an orange gel which was separated from the mother liquid by decantation. Trituration of the gel with ether afforded complex **3** as a dark yellow solid (92 mg, 87% yield). ^{1}H NMR (400 MHz, Acetone) δ 9.37 (dd, *J* = 18.7, 5.3 Hz, 2H, C*H*(6) bipy), 8.79 (d, *J* = 8.1 Hz, 2H, C*H*(3) bipy), 8.46 (t, *J* = 7.9 Hz, 2H, C*H*(4) bipy), 8.05 (s, 1H, C*H*(2)Im), 7.94 (dd, *J* = 7.1, 6.1 Hz, 2H, C*H*(5) bipy), 7.05 (s, 1H, C*H*(5)Im), 4.27 (s, 1H, CC*H*), 3.64 (s, 3H, C*H*3). ^{13}C NMR (101 MHz, Acetone) δ 157.7 (*C*(2) bipy), 155.7 (*C*(6) bipy), 143.3(*C*(2) M), 143.1 (*C*(4) bipy), 135.2 (*C*(4) Im), 130.7 (*C*(5) bipy), 126.8 (*C*(3) bipy), 89.8 (C*C*H), 70.7 (*C*CH), 34.5 (*C*H$_3$). *C*O and (*C*(5) Im) not observed. IR (solid, cm^{-1}, ν(CO)): 2025, 1918, 1894, MS ES *m/z*: calculated for $C_{18}H_{14}N_4O_3Re^+$ (M^+) 533.0, found 532.8. Elem. Anal. for $C_{20}H_{14}F_3N_4O_6PReS.CH_3CN$ required C, 36.56; H, 2.37; N, 9.69 %, found C,36.99 ; H, 2.22; N, 9.35%.

Complex 4: [Re(bipy)(CO)$_3$(CF$_3$SO$_3$)] (164 mg, 0.28 mmol) was added to a solution of imidazole (193 mg, 2.8 mmol) in DCM (10ml). The mixture was stirred for 48 h at room temperature under an argon atmosphere. Then, the volume of the reaction was reduced up to 2/3 under vacuum, and ether was added to force the precipitation of the desired product. **4** was obtained as a yellow solid (167 mg, 91 %).^{1}H NMR (400 MHz, CD_2Cl_2) δ 11.89 (s, br, 1H, N*H*), 9.10 (ddd, *J* = 5.5, 1.5, 0.8 Hz, 2H, C*H*(6) bipy), 8.32 (d, *J* = 8.2 Hz, 2H, C*H*(3) bipy), 8.28 – 8.19 (m, 2H, C*H*(4) bipy), 7.70 (ddd, *J* = 7.6, 5.5, 1.3 Hz, 2H, C*H*(5) bipy), 7.11 (s, 1H, C*H*(2)ImH), 6.93 (t, *J* = 1.4 Hz, 1H, C*H*(4)ImH), 6.72 (t, *J* = 1.4 Hz, 1H, C*H*(5)ImH).[14]

Complex 5: [Re(bipy)(CO)$_3$(CF$_3$SO$_3$)] (98 mg, 0.17 mmol) and [Au(C≡CPy-2)PPh$_3$] (120 mg, 0.21 mmol) were stirred in DCM (10 ml) for 72 h at room temperature under an argon atmosphere. Then, the solvent was removed under reduced pressure and methanol was added in order to precipitated the non-reacted pyridine derivative. The mixture was passed through celite and the solvent was removed again. The brownish slurry left was redisolved in THF and further addition of ether afforded the precipitation of **5** as a brownish solid (100 mg, 52 % yield) ^{1}H NMR (400 MHz, Acetone) δ 9.73 (dd, *J* = 5.5, 0.7 Hz, 2H, C*H*(6) bipy), 8.62 (d, *J* = 8.2 Hz, 2H, C*H*(3) bipy), 8.39 (td, *J* = 8.0, 1.5 Hz, 2H, , C*H*(4) bipy), 8.35 – 8.31 (m, 1H, , C*H*(6) py), 7.89 – 7.83 (m, 2H, C*H*(5) bipy), 7.80 (td, *J* = 7.8, 1.6 Hz, 1H, , C*H*(4) py), 7.77 – 7.61 (m, 15H, Ph), 7.51 (dd, *J* = 8.0, 0.7 Hz, 1H, C*H*(3) py), 7.19 (ddd, *J* = 7.5, 6.0, 1.5 Hz, 1H, , C*H*(5) py). ^{13}C NMR (101 MHz, Acetone) δ 196.5 (*C*O), 192.3 (*C*O), 157.1 (*C*(6) bipy), 156.8 (*C*(2) bipy), 152.5 (*C*(6) py), 148.6 (*C*(2) py), 142.1 (*C*(4) bipy), 139.9 (*C*(4) py), 135.2 (d, ^{2}J = 13.9 Hz, C*ortho*, ph), 133.1 (d, ^{4}J = 1.9 Hz C*para*, ph), 132.7 (*C*(3) py), 130.5 (d, ^{3}J = 11.4 Hz, C*meta*, ph), 130.0 (s, br, C*C*Au), 129.0 (*C*(5) bipy), 125.1, (*C*(3) bipy), 124.3 (*C*(5) py), 101.9 ((d, ^{3}J = 26 Hz, *CC*Au). C$_{ipso}$(Ph) not observed. ^{31}P NMR (162 MHz, Acetone) δ 41.54. IR (solid, cm^{-1}, ν(CO)): 2026, 1915, MS ES *m/z*: calculated for $C_{38}H_{38}AuN_3O_3PRe^+$ (M^+) 989.1, found 988.3. Elem. Anal. for $C_{39}H_{27}AuF_3N_3O_6PReS$, required C, 41.20; H, 2.39; N, 3.70 %, found C, 41.38; H, 2.62; N, 3.61%.

Complex 6: [Re(bipy)(CO)$_3$(CF$_3$SO$_3$)] (52 mg, 0.09 mmol) and [Au(C≡CPy-3)PPh$_3$] (51 mg, 0.09 mmol) were stirred in DCM (10 ml) for 12 h at room temperature under an argon atmosphere. Then, the volume of the reaction was reduced up to 1/3 under vacuum and ether was added to precipitate **6** as a yellow solid (45 mg, 44 % yield). ^{1}H NMR (400 MHz, Acetone) δ 9.54 (d, *J* = 4.8 Hz, 2H, C*H*(6) bipy), 8.76 (d, *J* = 8.2 Hz, 2H, C*H*(3) bipy), 8.48 (td, *J* = 8.0, 1.5 Hz, 2H, C*H*(4) bipy), 8.39 (d, *J* = 1.8 Hz, 1H, C*H*(2) py), 8.33 (d, *J* = 4.9 Hz, 1H, C*H*(6) bipy), 8.03 (ddd, *J* = 7.6, 5.5, 1.2 Hz, 2H, C*H*(5) bipy), 7.90 – 7.84 (m, 1H, C*H*(4) py), 7.72 – 7.56 (m, 15H, 3Ph), 7.36 (dd, *J* = 7.7, 6.0 Hz, 1H, C*H*(5) py). ^{31}P NMR (162 MHz, Acetone) δ 42.29. ^{13}C NMR (101 MHz, Acetone) δ 196.3 (*C*O), 192.4 (*C*O), 156.8 (*C*(2) bipy), 155.0 (*C*(6) bipy), 154.9 (*C*(2) py), 149.9 (*C*(6) py), 143.2 (*C*(4) py), 142.4 (*C*(4) bipy), 134.5 (d, ^{2}J = 13.8 Hz, C*ortho*, Ph), 132.9 (d, ^{4}J = 2.5 Hz, C*para*, Ph), 130.4 (d, ^{3}J = 11.4 Hz, C*meta*, Ph), 130.3 (d, J = 56.8 Hz, C*ipso*, Ph 130.0(*C*(5) bipy), 127.3 (*C*(5) py), 126.7 (*C*(3) py), 125.9 (*C*(3) bipy), 97.0 (s, br, *C*CAu). C*C*Au not observed. IR (solid, cm^{-1}, ν(CO)): 2028, 1903, ν(CC): 2121. MS ES *m/z*: calculated for $C_{38}H_{38}AuN_3O_3PRe^+$ (M^+) 989.1, found 988.4. Elemental analysis for

View Article Online
DOI: 10.1039/C4SC01684J

$C_{39}H_{27}AuF_3N_3O_6PReS.2H_2O$ required C, 39.44; H, 2.66; N, 3.58 %, found C, 39.8; H, 2.44; N, 3.82 %.

Complex 7: [Re(bipy)$(CO)_3(CF_3SO_3)$] (100 mg, 0.17 mmol) was added to a solution of [Au(C≡CImMe)PPh_3] (100 mg, 0.18 mmol) in DCM (5ml). The mixture was stirred for 12 h at room temperature under an argon atmosphere. Then, 2/3 of the solvent was removed under vacuum to afford an orange gel, which was triturated with ether to give complex **7** as an orange solid (92 mg, 54 %). ^{1}H NMR (400 MHz, Acetone) δ 9.38 – 9.29 (m, 2H, C*H*(6) bipy), 8.80 (d, *J* = 8.1 Hz, 2H, C*H*(3) bipy), 8.46 (td, *J* = 8.0, 0.8 Hz, 2H, C*H*(4) bipy), 8.01 – 7.91 (m, 2H, C*H*(5) bipy), 7.89 (s, 1H, C*H*(2)Im), 7.69 – 7.51 (m, 15H), 6.57 (s, 1H, C*H*(4)Im), 3.57 (s, 3H, CH_3). ^{13}C NMR (101 MHz, Acetone) δ 196.7 (*C*O), 192.9 (*C*O), 156.7 (*C*(2) bipy), 154.7 (*C*(6) bipy), 142.1 (*C*(4) bipy), 139.9 (C(2)Im), 135.0 (d, ^{2}J = 13.9 Hz, C*ortho*, Ph), 132.9 (s, br, C*para*, Ph), 131.0 (C(4)Im), 130.0 (s, br, C*C*Au), 130.4 (d, ^{3}J = 11.3 Hz, C*meta*, Ph), 129.7 (*C*(5) bipy) , 125.8 (*C*(3) bipy), 121.5 (C(5)Im), 86.9 (d, ^{3}J = 21.6 Hz, *C*CAu), 33.1 (*C*H_3). C_{ipso}(Ph) not observed. ^{31}P NMR (162 MHz, Acetone) δ 42.19. IR (solid, cm^{-1}, υ(CO)): 2025, 1930, 1893 MS ES *m/z*: calculated for $C_{37}H_{28}AuN_4O_3PRe^+$ (M^+) 991.1, found 990.9. Elem. Anal. for $C_{38}H_{28}AuF_3N_4O_6PReS$ required C, 40.04; H, 2.48; N, 4.92 %, found C, 39.46; H, 2.44; N 4.99 %

Complex 8: KOH (6.5 mg, 0.11 mmol) dissolved in MeOH (2 ml) was added dropwise to a solution of **4** (50 mg, 0.07 mmol) and [AuClPPh_3] (42 mg, 0.08 mmol) in THF (5ml). The mixture was stirred at room temperature under an argon atmosphere for 1 hour. Then, the bulk reaction was filtered through celite to eliminate the KCl formed during the reaction and the volume of the reaction was reduced until 1/3 under vacuum. Further addition of ether forced the precipitation of complex **8** as a yellow solid (75 mg, 88 % yield)**.** ^{1}H NMR (400 MHz, CD_2Cl_2) δ 9.09 (ddd, *J* = 5.5, 1.6, 0.8 Hz, 2H, C*H*(6) bipy), 8.61 (dd, *J* = 7.3, 0.9 Hz, 2H, C*H*(3) bipy), 8.31 – 8.25 (m, 2H, C*H*(4) bipy), 7.67 (ddd, *J* = 7.7, 5.5, 1.2 Hz, 2H, C*H*(5) bipy), 7.62 – 7.55 (m, 3H, C*H*(*para*) Ph), 7.54 – 7.46 (m, 12H, C*H*(*ortho, meta*) Ph), 7.16 (t, *J* = 1.0 Hz, 1H, C*H*(2)Im), 6.78 (t, *J* = 1.2 Hz, 1H, C*H*(Im)), 6.41 (t, *J* = 1.2 Hz, 1H, C*H*(Im)). ^{31}P NMR (162 MHz, CD_2Cl_2) δ 31.18. ^{13}C NMR (101 MHz, CD_2Cl_2) δ 197.3 (*C*O), 192.8(*C*O), 156.3 (*C*(2) bipy), 153.4 (*C*(6) bipy), 144.2 (*C*(2) Im), 141.4 (*C*(4) bipy), 134.7 (d, ^{2}J = 13.5 Hz, C*ortho*, ph) 132.9 (d, ^{4}J = 2.2 Hz, C*para*, ph), 130.0 (d, ^{3}J = 11.9 Hz, C*ortho*, ph), 128.7 (*C*(5) bipy), 127.0 (C(Im)), 126.8, (C(Im)), 125.41 (*C*(3) bipy). C_{ipso}(Ph) not observed. IR (solid, cm^{-1}, ν(CO)): 2020, 1921, 1892-. MS ES *m/z*: calculated for $C_{34}H_{24}AuN_4O_3PRe^+$ (M^+) 953.1, found 952.8. Elem. Anal. for $C_{35}H_{26}AuF_3N_4O_6PReS$ required C, 38.15; H, 2.38; N, 5.08 %, found C, 38.52; H, 2.56; N, 4.94 %.

View Article Online
DOI: 10.1039/C4SC01684J

Journal Name RSCPublishing

Table 4 X-ray crystallographic data of complexes **2**, **5**, **7** and **8**.

Compound	2	5	7	8
Formula	$C_{21}H_{13}N_3F_3O_3RePS$	$C_{41}H_{33}AuF_6N_3O_4P_2Re$	$C_{21}H_{13}F_3N_3O_6ReS$	$C_{37}H_{26}AuN_4F_3O_{6.5}RePS$
M_r	678.62	1190.81	1139.86	1133.81
Crystal size (mm)	0.42 × 0.20 × 0.18	0.42 × 0.18 × 0.04	0.44 x 0.14 x 0.04	0.36 × 0.34 × 0.22
Crystal system	Monoclinic	Triclinic	Triclinic	Triclinic
Space group	P2(1)/n	P-1	P-1	P-1
Cell constants:				
a (Å)	13.1254(2)	9.46830(10)	8.9054(4)	13.0494(2)
b (Å)	13.0009(2)	16.4296(2)	9.0770(5)	13.4519(2)
c (Å)	13.7872(2)	29.0868(3)	22.9630(8)	22.5256(4)
α (°)	90	92.4970(10)	84.156(4)	95.9470(10)
β (°)	109.269(2)	92.6600(10)	88.572(3)	99.8470(10)
γ (°)	90	91.2060(10)	88.527(4)	102.1570(10)
V (Å^3)	2220.88(6)	4748.77(8)	1845.48(15)	3768.28(10)
Z	4	4	2	4
*D*x (Mg m^{-3})	2.030	1.954	2.051	1.999
μ(mm^{-1})	5.636	6.759	7.415	7.264
F(000)	1304	2280	1088	2160
T (K)	100(2)	100(2)	100(2)	173(2)
$2\theta_{max}$	51	51	51	51
No. of refl.:				
Measured	21904	60411	27131	72134
Independent	4116	15009	6799	13940
Transmissions	0.4303 – 0.2006	0.7738 - 0.1635	0.7558-0.1388	0.2979 – 0.1796
R_{int}	0.0215	0.0429	0.0664	0.0299
Parameters	316	1049	227	982
Restraints	0	0	0	0
Goodness of fit on F^2	1.085	1.037	1.142	1.103
wR(F^2, all Refl.)	0.0352	0.0641	0.2280	0.0551
R(I >2σ(I))	0.0144	0.0272	0.0873	0.0244
max. Δρ (e Å^{-3})	0.871	1.212	7.266	1.155

Conclusions

In the search of new anti-cancer and diagnosis agents, two new families of luminescent *fac*-$[Re(bipy)(CO)_3(L)]^+$ and *fac*-$[Re(bipy)(CO)_3(L\text{-}AuPPh_3)]^+$, where L is an imidazole, alkynyl-imidazole or alkynyl-pyridine derivative, have been synthesised and characterised. Cytotoxicity studies performed in human A549 lung cancer cells revealed that the heterometallic Re(I)/Au(I) derivatives presented values of IC_{50} more than 10 times lower than their analogous Re(I) complexes. In addition, among the heterometallic species, the presence of alkynyl groups increases the toxicity of the bioprobes. Although this statement is made by comparison of three alkynyl species, complexes **5**, **6** and **7**, with the single species lacking of an alkynyl group, complex **8**, it agrees with published reports that support the same idea.[4,6] These results revealed the feasibility of easily modulate the cytotoxicity of

View Article Online
DOI: 10.1039/C4SC01684J

the probes upon their chemical structure, reaching their maximum cytotoxic effect when an alkynyl group and a phosphine gold fragment are brought together. Moreover, fluorescence cell imaging pointed out the different bio-distribution as well as uptake level depending on the concentration loadings and nature of the probes. Therefore, whereas rhenium species **1-4** followed the typical biodistribution of monocationic rhenium species, *i.e.* general cytoplasmatic staining and likely mitochondrial localisation, the heterometallic Re(I)/Au(I) species **5-8** displayed a more intense luminescence suggesting a higher uptake level and a complicated localisation pattern. Loadings at concentrations beyond their IC_{50} value promoted a high uptake level possibly due to the disruption of the cell membrane. Then, accumulation in the nucleus and nucleolus, where proteins are concentrated, could be proposed because of the great affinity of Au(I) species for S donor ligands. The exact mechanism according to which these heterometallic species present such behaviour is not clear. The reaction with thiol residues (RSH) could afford either (*fac*-[Re(bipy)$(CO)_3$(L-Au-SR)]$^+$) species, if the phosphine fragment is displaced by the thiol residue or (*fac*-[Re(bipy)$(CO)_3$(L)]$^+$) and (RS-Au-PR_3), if the alkynyl group is displaced instead. Taking in mind that the bond length of Au-P is longer than Au-C, which can be used as an indication of bond strength, and also knowing that photoelectron spectroscopy measurements together with theoretical studies have shown that the Au-C bond in Au-alkynyl complexes represent one of the strongest gold-ligand bonds,[32] the formation of -[Re(bipy)$(CO)_3$(L-Au-SR)]$^+$) seems to be more likely. Moreover, the nucleous and nucleolus remained lighted up during the experiment, which suggest that the fragment of the bioprobe providing the luminescence remains trapped. Again, the mechanism where -[Re(bipy)$(CO)_3$(L-Au-SR)]$^+$) is formed seemed to be the expected as nothing would prevent (*fac*-[Re(bipy)$(CO)_3$(L)]$^+$) to leave the nucleus and nucleolus. In contrast, loadings at concentrations below their IC_{50} revealed a possible mitochondrial localisation. This result is in agreement with the affinity of Au(I) inhibiting the mitochondrial thioredoxin reductase. The same mechanism than the one described previously can be proposed for the interaction with the thioredoxin reductase. In view of this results, it could be postulated that (*fac*-[Re(bipy)$(CO)_3$(L-)]$^+$) fragment emerges not only as an excellent luminescent associate, able to light up the cell, but also can easily host bioactive species without interfering in biological role and allowing to visualise their biodistribution. Moreover, the synthetic feasibility of alkynyl gold complexes together with their demonstrated bioactivity opens a wide variety of possibilities for the design of more sophisticated heterometallic bioprobes. Although these are preliminary results and no other reports dealing with the biological aspects of heterometallic alkynyl Re(I)/Au(I) species have been published yet, there is a remarkable future for these type of heterometallic complexes. The synergy effect attained by the luminescent rhenium fragment (*fac*-[Re(bipy)$(CO)_3$(L-)]$^+$) and the bioactive gold fragment (-C≡CAuPPh_3) is unique and crucial in order to consider Re(I)/Au(I) species as cooperative partners in the fields of drug biodistribution, visualization and cancer therapy.

Acknowledgements

Authors thank the Ministerio de Economía y Competitividad (MINECO/FEDER CTQ2010-20500-C02-01 and SAF2010-14920) and DGA-FSE (E77 and B16) for financial support and J. M. López-de-Luzuriaga for lifetime measurements.

Notes and references

[a] Departamento de Química Inorgánica, Instituto de Síntesis Química y Catálisis Homogénea (ISQCH), Universidad de Zaragoza-CSIC, E-50009 Zaragoza, Spain. E-mail: gimeno@unizar.es; Fax: +34 976761187; Tel: +34 976762291 and vanesa@unizar.es; Tel: +34 976763523.
[b] Departamento de Bioquímica y Biología Celular, Universidad de Zaragoza, E-50009 Zaragoza, Spain.

†Electronic supplementary information (ESI) available: Structural features secondary interactions and hydrogen bonds of **5** and **8** (Fig. S1–S3); UV-Vis and emission spectra of complexes **1**, **3**-**5**, **7** and **8** (Fig. S4); Annexin-V analysis graph of complexes **1**-**8** (Fig. S5); Cell morphology pictures of complexes **1**-**8**. (Fig. S6); CCDC 996045–996048.

1 E. R. T. Tiekink, *Inflammopharmacology*, 2008, **16**, 138.
2 (*a*) I. Ott, *Coord. Chem. Rev.*, 2009, **253**, 1670; (*b*) B. Bertrand and A. Casini, *Dalton trans.*, 2014, **43**, 4209.
3 (*a*) L. Ortego, F. Cardoso, S. Martins, M. F. Fillat, A. Laguna, M. Meireles, M. D. Villacampa and M. C. Gimeno, *J. Inorg. Biochem.,* 2014, **130**, 32; (*b*) M. P. Rigobello, L. Messori, G. Marcon, M. A. Cinellu, M. Bragadin, A. Folda, G. Scutari, A. Bindoli, *J. Inorg. Biochem.*, 2004, **10**, 1634; (*c*) P. J. Barnard, S. J. Berners-Price, *Coord. Chem. Rev.,* 2007, **251** 1889; (*d*) K. Yan, C.-N. Lok, K. Bierlab and C.-M. Che, *Chem. Commun.,* 2010, **46**, 7691; (*e*) E. Vergara, A. Casini, F. Sorrentino, O. Zava, E. Cerrada, M. P. Rigobello, A. Bindoli, M. Laguna and P. J. Dyson, *ChemMedChem*, 2010, **5**, 96; (*f*) V. Gandin, A. P. Fernandes, M. P. Rigobello, B. Dani, F. Sorrentino, F. Tisato, M. Björnstedt, A. Bindoli, A. Sturaro, R. Rella and C. Marzano, *Biochem. Pharmacol*, 2010, **79**, 90; (*g*) J. L. Hickey, R. A. Ruhayel, P. J. Barnard, M. V. Baker, S. J. Berners-Price and A. Filipovska**,** *J. Am. Chem. Soc.*, 2008, **130**, 12570; (*h*) S. Urig, K. Fritz-Wolf, R. Réau, C. Herold-Mende, K. Tóth, E. Davioud-Charvet and K. Becker, *Angew. Chem. Int. Ed.,* 2006, **45**, 1881.
4 D.-L. Ma, T. Y.-T. Shum, F. Zhang, C.-M. Che and M. Yang, *Chem. Commun.*, 2005, 4675.
5 J. C. Lima and L. Rodriguez, *Anticancer Agents Med. Chem.*, 2011, **11**, 921.
6 (*a*) A. Meyer, A. Gutiérrez, I. Ott and L. Rodriguez, *Inorg. Chim. Acta*, 2013, **398**, 72; (*b*) A. Meyer, C. P. Bagowski, M. Kokoschka, M. Stefanopoulou, H. Alborzinia, S. Can, D. H. Vlecken, W. S. Sheldrick S. Wölfl and I. Ott, *Angew. Chem. Int. Ed.*, 2012, **51**, 8895; (*c*) R. G. Balasingham, C. F. Williams, H. J. Mottram, M. P. Coogan and S. J. A. Pope, *Organometallics*, 2012, **31**, 5835; (*d*) E. Vergara, E. Cerrada, A. Casini, O. Zava, M. Laguna and P. J. Dyson, *Organometallics*, 2010, **29**, 2596; (*e*) C.-H. Chui, R. S.-M. Wong, R. Gambari, G. Y.-M. Cheng, M. C.-W. Yuen, K.-W. Chan, S.-W. Tong, F.-Y. Lau, P. B.-S. Lai, K.-H. Lam, C.-L. Ho, C.-W. Kan, K.

S.-Y. Leung and W.-Y. Wong, *Bioorg. Med. Chem*., 2009, **17**, 7872; (*f*) E. Schuh, S. M. Valiahdi, M. A. Jakupec, B. K. Keppler, P. Chiba and F. Mohr, *Dalton Trans.*, 2009, 10841.

7 (*a*) D.-L. Ma, C.-M. Che, F.-M. Siu, M. Yang and K.-Y. Wong, *Inorg. Chem.*, 2007, **46**, 740; (*b*) A. V. Shtemenko, P. Collery, N. I. Shtemenko, K. V. Domasevitch, E. D. Zabitskayac and A. A. Golichenkoa, *Dalton Trans*., 2009, 5132; (*c*) S. Wirth, A. U. Wallek, A. Zernickel, F. Feil, M. Sztiller-Sikorska, K. Lesiak-Mieczkowska and C. Braüchle, *J. Inorg. Biochem*., 2010, **104**, 774; (*d*) J. Martínez-Lillo, T. F. Mastropietro, R. Lappano, A. Madeo, M. E. Alberto, N. Russo, M. Maggiolini and G. De Munno, *Chem. Commun.*, 2011, **47**, 5283; (*e*) M. D. Bartholoma, A. R. Vortherms, S. Hillier, B. Ploier, J. Joya, J. Babich, R. P. Doyle and J. Zubieta, *ChemMedChem*, 2010, **5**, 1513.

8 (*a*) L. A. Sacksteder, M. Lee, J. N. Demas and B. A. DeGraff, *J. Am. Chem. Soc.*, 1993, **115**, 8230; (*b*) D. J. Stufkens and Jr. A. Vlček, *Coord. Chem. Rev.*, 1998, **177**, 127; (*c*) F. L. Thorp-Greenwood, J. A. Platts, and M. P. Coogan, *Polyhedron*, 2014, **67**, 505; (*d*) K. E. Henry, R. G. Balasingham, A. R. Vortherms, J. A. Platts, J. F. Valliant, M. P. Coogan, J. Zubieta and R. P. Doyle, *Chem. Sci.,* 2013, **4**, 2490

9 (*a*) V. Fernández-Moreira, F. L. Thorp-Greenwood and M. P. Coogan, *Chem. Commun*., 2010, **46**, 186; (*b*) K. K.-W. Lo, M.-W. Louie and K. Y. Zhang, *Coord. Chem. Rev*., 2010, **254**, 2603; (*c*) F. L Thorp-Greenwood, *Organometallics*, 2012, **31**, 5686; (*d*) M. P. Coogan and V. Fernández-Moreira, *Chem. Commun*., 2014, **50**, 384.

10 (*a*) V. Fernández-Moreira, M. L. Ortego, C. F. Williams, M. P. Coogan, M. D. Villacampa and M. C. Gimeno, *Organometallics*, 2012, **31**, 5950; (*b*) A. J. Amoroso, R. J. Arthur, M. P. Coogan, J. B. Court, V. Fernández-Moreira, A. J. Hayes, D. Lloyd, C. O. Millet and J. A. Pope, *New J. Chem.* 2008, **32**, 1097; (*c*) V. Fernández-Moreira, F. L. Thorp-Greenwood, A. J. Amoroso, J. Cable, J. B. Court, V. Gray, A. J. Hayes, R. L. Jenkins, B. M. Kiriuki, D. Lloyd, C. O. Millet, C. F. Williams and M. P. Coogan, *Org. Biomol. Chem.* 2010, **8**, 3888; (*d*) A. J. Amoroso, M. P. Coogan, J. E. Dunne, V. Fernández-Moreira, J. B. Hess, A. J. Hayes, D. Lloyd, C. O. Millet, J. A. Pope and C. Williams, *Chem Commun.*, 2007, 3066; (*e*) K. K.-W. Lo, M.-W. Louie, K.-S. Sze and J. S.-Y. Lau, *Inorg. Chem.*, 2008, **47**, 602; (*f*) M.-W. Louie, M. H.-C. Lam and K. K.-W. Lo, *Eur. J. Inorg. Chem.,* 2009, 4265; (*g*) K. K.-W. Lo, M.-W. Louie, K. Y. Zhang and S. P.-Y. Li, *Eur. J. Inorg. Chem.*, 2011, 3551. (*f*) E. E. Langdon-Jones, N. O. Symonds, S. E. Yates, A. J. Hayes, D. Lloyd, R. Williams, S. J. Coles, P. N. Horton and S. J. A. Pope, *Inorg. Chem.*, 2014, **53**, 3788.

11 (*a*) K.-L. Cheung, S.-K. Yip and V. W.-W. Yam, *J. Organomet. Chem.,* 2004, **689**, 4451; (*b*) Y. Yamamoto, M. Shiotsuka and S. Onaka, *J. Organomet. Chem.,* 2004, **689**, 2905; (*c*) M. Ferrer, L. Rodríguez, O. Rossell, J. C. Lima, P. Gómez-Sal and A. Martin, *J. Organomet. Chem*., 2004, **23**, 5096.

12 (*a*) R. H. Naulty, M. P. Cifuentes, M. G. Humphrey, S. Houbrechts, C. Boutton, A. Persoons, G. A. Heath, D. C. R. Hockless, B. Luther-Daviesa and M. Samoc*, J. Chem. Soc*., *Dalton Trans*., 1997, 4167; (*b*) M. C. Blanco, J. Cámara, M. C. Gimeno, P. G. Jones, A. Laguna, J. M. López-de-Luzuriaga, M. E. Olmos and M. D. Villacampa, *Organometallics,* 2012, **31**, 2597; (*c*) D. Emeljanenko, E. Kaifer and H.-J. Himmel, *Eur. J. Inorg. Chem.*, 2011, 2975.

13 (*a*) J. V. Caspar and T. J. Meyer, *J. Phys. Chem.*, 1983, **87**, 952; (*b*) J. K. Hino, L. D. Ciana, W. J. Dressick and B. P. Sullivan, *Inorg. Chem.*, 1992, **31**, 1072; (*c*) Y. Wang, L. A. Lucia and K. S. Schanze, *J. Phys. Chem.*, 1995, **99**, 1961.

14 E. Gómez, M. A. Huertos, J. Pérez, L. Riera and A. Menéndez-Velázquez, *Inorg. Chem*., 2010, **49,** 9527.

15 S. V. Wallendael, R. J. Shaver, D. P. Rillema, B. J. Yoblinski, M. Stathis and T. F. Guarr, *Inorg. Chem.*, 1990, **29**, 1761.

16 (*a*) K. Nomiya, R. Noguchi, K. Ohsawa, K. Tsuda and M. Oda, *J. Inorg. Biochem.,* 2000, **78**, 363; (*b*) K. Nomiya, K. Tsuda, Y. Tanabe, H. Nagano, *J. Inorg. Biochem.,* 1998, **69**, 9.

17 (*a*) M. Iglesias and M. Albrecht, *Dalton Trans.*, 2010, **39**, 5213; (*b*) A. A. Tukov, A. T. Normand and M. S. Nechaev, *Dalton Trans.*, 2009, 7015.

18 (a) D. M. Dattelbaum, K. M. Omberg, J. R. Schoonover, R. L. Martin and T. J. Meyer, *Inorg. Chem.*, 2002, **41**, 6071; (b) B. S. Uppal, R. K. Booth, N. Ali, C. Lockwood, C. R. Rice and P. I. P. Elliot, *Dalton Trans.,* 2011, **40**, 7610.

19 V. W.-W. Yam and S. W.-K. Choi, *J. Chem. Soc.*, *Dalton Trans.,* 1996, 4227.

20 W. B. Connick, A. J. Di Bilio, M. G. Hill, J. R. Winkler and H. B. Gray, *Inorg. Chim. Acta,* 1995, **240**, 169.

21 (*a*) M. I. Bruce and D. N. Duffy, *Aust. J. Chem.*, 1986, **39**, 1697; (*b*) J. Vicente, J. Gil-Rubio, N. Barquero, P. G. Jones and D. Bautista, *Organometallics,* 2008, **27***,* 646.

22 (*a*) L. Sacksteder, A. P. Zipp, E. A. Brown, J. Streich, J. N. Demas and B. A. DeGraff, *Inorg. Chem.*, 1990, **29**, 4335; (*b*) J. V. Caspar, B. P. Sullivan and T. J. Meyer, *Inorg. Chem.*, 1984, **23**, 2104.

23 E. García-Moreno, S. Gascón, M. J. Rodríguez-Yoldi, E. Cerrada, and M. Laguna, *Organometallics*, 2013, **32**, 3710.

24 A. Gutiérrez, M. C. Gimeno, I. Marzo and N. Metzler-Nolte, *Eur. J. Inorg. Chem.,* 2014, 2512.

25 (*a*) K. Y. Zhang, K. K.-S. Tso, M.-W. Louie, H.-W. Liu and K. K.-W. Lo, *Organometallics*, 2013, **32**, 5098; (*b*) T. S. Pitchumony, L. Banevicius, N. Janzen, J. Zubieta and J. F. Valliant, *Inorg. Chem.,* 2013, **52**, 13521.

26 M.-W. Louie, H.-W. Liu, M. H.-C. Lam, T.-C. Lau and K. K.-W. Lo, *Organometallics*, 2009, **28**, 4297.

27 S. Gromer, S. Urig, K. Becker, *Med. Res. Rev.*, 2004, **24**, 40.

28 C. P. Bagowski, Y. You, H. Scheffler, D. H. Vlecken, D. J. Schmitz and I. Ott, *Dalton Trans.*, 2009, 10799.

29 E. J. New and D. Parker, *Org. Biomol. Chem.,* 2009, **7**, 851.

30 (*a*) R. A. Poole, G. Bobba, J.-C. Frias, M. J. Cann and D. Parker, *Org. Biomol. Chem*., 2005, **3**, 1013; (*b*) J. Yu, R. Pal, R. A. Poole, M. J. Cann and D. Parker, *J. Am. Chem. Soc.*, 2006, **128**, 2294; (*c*) R. Pal and D. Parker, *Org. Biomol. Chem.*, 2008, **6**, 1020.

31 G. M. Sheldrick, *Acta Cryst.*, 2008, **A64**, 112.

32 H.-T. Liu, X.-G. Xiong, P. D. Dau, Y.-L. Wang, D.-L. Huang, J. Liand and L.-S. Wang, *Nat. Commun.* 2013, **4**, 2201.

